



OPEN Characteristic mode analysis of electromagnetic interference susceptibility in motor driven unmanned drones for enhanced design and performance

Peyman Hasani¹, Seyed Mohamad Hashemi¹✉, Alireza Sadeqi¹, Javad Ghalibafan² & Valiollah Mashayekhi²

The rapid advancement of portable device technology, especially in the realms of drones and motor-driven systems, underscores the critical need for thorough analysis of Electromagnetic Interference (EMI) to guarantee operational reliability and safety. These systems' vulnerability to EMI can result in diminished performance and heightened safety concerns, making it essential to evaluate their susceptibility. This research explores how brushless and brushed motors respond to EMI through Characteristic Mode Analysis (CMA), pinpointing significant frequency modes—2.1 GHz, 2.92 GHz, and 2.98 GHz—that impact motor functionality differently, with Mode 1 at 2.1 GHz being the most significant. Due to constraints in testing capabilities, the study focused on radiation exposure at 2.45 GHz. Experiments conducted with a 22 kW electromagnetic source revealed that as the motor neared the source, disruptions increased, culminating in total motor failure at a distance of 0.6 m. Additionally, the extensive wiring connected to the motor intensified damage by inducing extra currents, thereby amplifying the motor's susceptibility beyond that of direct radiation exposure. The results of this study demonstrate the effectiveness of CMA in forecasting EMI effects and offer critical insights into the vulnerabilities present in motor-driven systems. By identifying the relevant radiation frequency, pattern, and power density that contribute to component damage, proactive measures can be taken to shield electronic components from adverse environmental conditions characterized by these factors.

The rapid advancement of portable technology, particularly in drones utilized for surveillance, delivery, and exploration, alongside motor-driven systems critical to automotive, manufacturing, and robotics, necessitates a heightened focus on ensuring system reliability and safety. A significant challenge in these domains is assessing the vulnerability of sensitive components, such as motors and propulsion systems, to electromagnetic interference (EMI). This vulnerability involves key characteristics like radiation patterns, emission direction, and power density. For instance¹, reported that high-power electromagnetic (HPEM) pulses significantly impact Unmanned Aerial Vehicle sensor systems by interfering with motor control signals, leading to fluctuations in motor speed and vibrations that compromise sensor accuracy. Moreover², found that electromagnetic wave coupling in quadcopter drones predominantly occurs through the power cables connecting the printed circuit board to the motors.

EMI can originate from various sources and poses the risk of disrupting device functionality, resulting in operational inefficiencies and potential system failures. EMI can be classified into two categories: high power and low power. High power EMI encompasses intense electromagnetic signals capable of severely damaging electronic devices, typically with field intensities exceeding 100 V/m³. This category includes diverse methods applicable to drones, such as high-frequency jamming and laser-induced interference, which can lead to significant operational failures. Further investigations into the effects of HPEM pulses are detailed in⁴. In contrast, low power EMI employs weaker signals to disrupt devices by targeting their operational mechanisms, including techniques such as antenna coupling for analog sensors⁵ and bulk current or direct power injection

¹Faculty of Electrical Engineering, Shahid Rajaee Teacher Training University, Tehran, Iran. ²Department of Electrical Engineering, Shahrood University of Technology, Shahrood, Iran. ✉email: sm.hashemi@sru.ac.ir

for digital sensors⁶. For RF communication modules, in-band jamming is an effective low-power approach when channel information is available. Additionally, non-RF interference, such as acoustic⁷ and light signals⁸, can exert significant impacts under appropriate conditions.

Given the complexities of EMI, effective analytical techniques are essential for comprehensively understanding its effects on portable devices. To achieve efficient power coupling within a circuit, selecting appropriate resonant frequencies is crucial. Historically, various techniques have been employed, including measuring coupled power through frequency sweeping⁹, identifying frequencies with a high radar cross-section (RCS)², and conducting near-field scanning to analyze electric field distribution¹⁰. The frequency sweep method⁹ involves gradually varying the frequency of an input signal and measuring the system's response to identify resonance characteristics. This technique is effective for determining the resonance frequency of various systems, including mechanical and electrical devices. However, it requires specialized equipment, such as a Vector Network Analyzer (VNA), and can be time-consuming due to the need for precise measurements across a range of frequencies. This complexity and resource intensity can limit its practicality in some applications. Furthermore, in², the determination of critical resonance frequencies relies on impedance measurements via VNA, as well as Radar Cross Section (RCS) and inverse synthetic aperture radar imaging. These methods demand resource-intensive experimental setups, such as anechoic chambers, and involve prolonged measurement cycles. In¹⁰, near-field scanning was utilized to map the electric-field distribution of a compact flight-controller board. This approach employed a spectrum analyzer, a shielded environment, and precision probes to identify frequencies with elevated field magnitudes. While this non-invasive method enables the prediction of interference susceptibility by correlating near-field hotspots with induced current changes, it remains equipment-intensive and time-consuming due to the need for high-resolution spatial scanning and extensive post-processing.

Due to the challenges mentioned, the need for the CMA method, which is available in full wave software's, becomes prominent. CMA can streamline the investigation of electromagnetic coupling and interference in portable device systems, offering a more efficient alternative to traditional techniques.

Characteristic Mode Analysis (CMA) decomposes induced currents within a device into orthogonal modes, each characterized by unique resonance properties such as eigenvalues and eigenvectors. This modal decomposition not only facilitates a detailed understanding of the device's resonant behavior but also enables targeted analysis of EMI effects with enhanced efficiency^{11,12}. For instance, researchers have utilized CMA to examine the fundamental modes of basic drone configurations, while neglecting the motor structure¹³ and simplified systems¹⁴.

In this study, we leverage CMA to investigate radiation characteristics that may impact the performance of portable devices, with a particular focus on motors used in drones. Unlike previous studies, such as¹³, which analyze only a basic and abstracted structure of drones while neglecting the motor structure, our work provides a comprehensive and detailed analysis of brushless DC motors (BLDC). We examine critical design elements, including stator slots, rotor configurations, cooling systems, and wiring, to understand their impact on EMI susceptibility. By identifying fundamental modes and resonant frequencies (e.g., 2.1 GHz, 2.92 GHz, and 2.98 GHz), we pinpoint critical factors such as polarization, frequency, and power density of electromagnetic radiation that pose potential risks to motor performance.

This approach not only streamlines analytical procedures but also enhances design methodologies, ensuring that portable devices are resilient to EMI challenges. Importantly, our findings are not limited to BLDC motors but are also applicable to brushed motors, ensuring broader relevance and impact. By integrating CMA with full-wave simulations and experimental validation, we provide actionable insights for designing motors with minimal EMI susceptibility, addressing a critical gap in prior research.

In Sect. 2, we explore the influence of motor design parameters on CMA, employing advanced simulation techniques tailored for portable devices. Section 3 presents our findings from EMI analysis, emphasizing various modes and their implications across different frequencies and polarizations, thereby substantiating CMA outcomes with comprehensive simulations. In Sect. 4, we analyze the measurement results obtained from the Phantom 4 drone motor. Finally, Sect. 5 concludes with insights into future research directions and practical applications for identifying the impact of EMI on electronic components in portable device systems.

Through this exploration, we underscore the effectiveness of CMA in predicting EMI in portable device applications, particularly in enhancing motor reliability and operational safety amidst electromagnetic complexities. Based on the thorough examination of the motor in this study, similar investigations can be conducted for other electronic components, such as sensors or communication modules in drones and mobile devices, to ensure that they are not exposed to specific environmental conditions that pose a high risk of damage.

The influence of motor design parameters on CMA

Drones and portable devices commonly use two types of motors: BLDC and brushed, as shown in Fig. 1. Brushless motors, which use electronic commutation, offer greater efficiency, durability, and power output compared to brushed motors that rely on mechanical brushes. The frictionless operation of brushless motors results in reduced heat generation and extended lifespan, although they are more complex and costly due to the need for electronic speed controllers. In contrast, brushed motors are simpler and more affordable but less efficient and require more frequent maintenance. Given their superior performance, reliability, and efficiency, brushless motors are preferred for high-performance drones and portable devices, while brushed motors are often used in more budget-friendly or entry-level applications^{15,16}. Brushless motors use electronic commutation and can be configured as either outrunner or inrunner types. Outrunner motors, where the rotor surrounds the stator, provide higher torque and efficiency, making them ideal for applications like drones. Inrunner motors, with the rotor inside the stator, are better suited for high-speed applications. Among brushless motors, outrunner types are more commonly used in drones due to their superior torque and effectiveness in lifting and stabilizing, making them the preferred choice for such applications^{15,16}. Table 1 lists the physical specifications of brushless

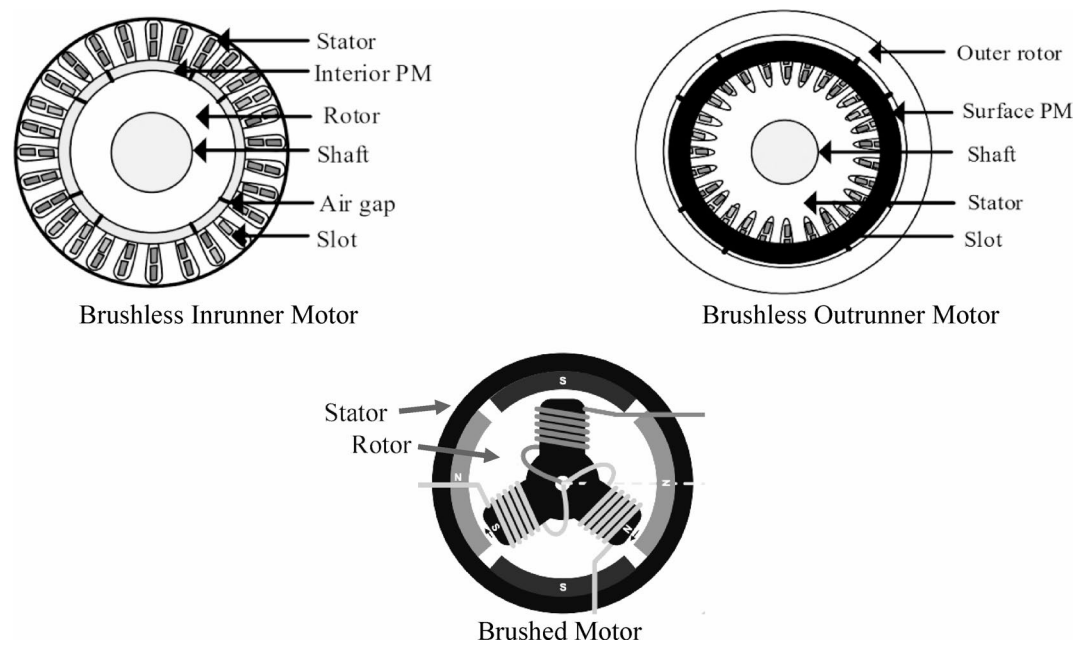


Fig. 1. The structure of three type of motors used in drones and portable devices.

Drone Name	Stator dimensions (D×H) (mm)	Rotor dimensions (D×H) (mm)	Slot number	Pole number
DJI Mavic 3 Pro	23 × 12	25 × 16	12	14
Autel Robotics EVO Lite+	22 × 6	25 × 11	12	14
Parrot Anafi	14 × 6	16 × 9	9	12
Yuneec Typhoon h Pro	22 × 13	25 × 19	12	14
DJI Air 2 S	23 × 12	25 × 13	12	14
Phantom 4	23 × 12	28.2 × 26	12	14

Table 1. List of physical specifications for commercial and industrial drone Motors.

motors used in industrial and commercial drones. The motor of the Phantom 4 drone has been designed and simulated as a case study, and this simulation approach can also be applied to other drone motors. It is essential to recognize that although the internal winding configurations of brushed and brushless motors differ, this distinction does not affect the CMA. Instead, the structural characteristics of the motor body, particularly the presence of slots, are the primary factors influencing the analysis. This allows for a consistent evaluation of various motor designs under EMI conditions, as different motor structures can be analyzed in a similar manner.

The motor has been simulated in five stages, with each stage incorporating additional design details. The analysis was conducted using CMA, and the simulations were performed using FEKO 2023 simulation software¹⁷. The aim of examining the impact of design details on CMA analysis results is to enable the prediction of outcomes for other motors with different configurations. The impact of each design modification is illustrated in the modal significant (MS) graph presented in Fig. 2. As shown in the figure, the inclusion of the rotor and shunt in Structure 2 has raised the MS graph. Adding the stator slots in Structure 3 introduced resonance at a frequency of 3.2 GHz. The addition of the upper and lower motor covers in Structure 4 shifted the resonance to 3.1 GHz, with minimal impact. Finally, the integration of the motor cooling system significantly affected the results, introducing resonance frequencies at 2.1, 2.92, and 2.98 GHz.

Determining the characteristics of EMI for maximum impact on the structure with CMA and validating the results using the full wave method

In this section, the detailed results for the motor structure, as depicted in Fig. 3, are presented. Table 2 outlines the dimensions of the various design parameters.

Based on the results from the previous section and as illustrated in Fig. 4, the resonance frequencies for the structure shown in Fig. 3 are found at 2.1, 2.92, and 2.98 GHz. These frequencies correspond to high values above 0.9 in the MS diagram and the points where the phase characteristic curve intersects 180 degrees.

This section explores how the structure is influenced by EMI. First, the radiation patterns for these three frequency modes are analyzed in both theta and phi polarizations, with the maximum E-field magnitude states recorded at 17 dBV. Figure 5 displays these patterns:

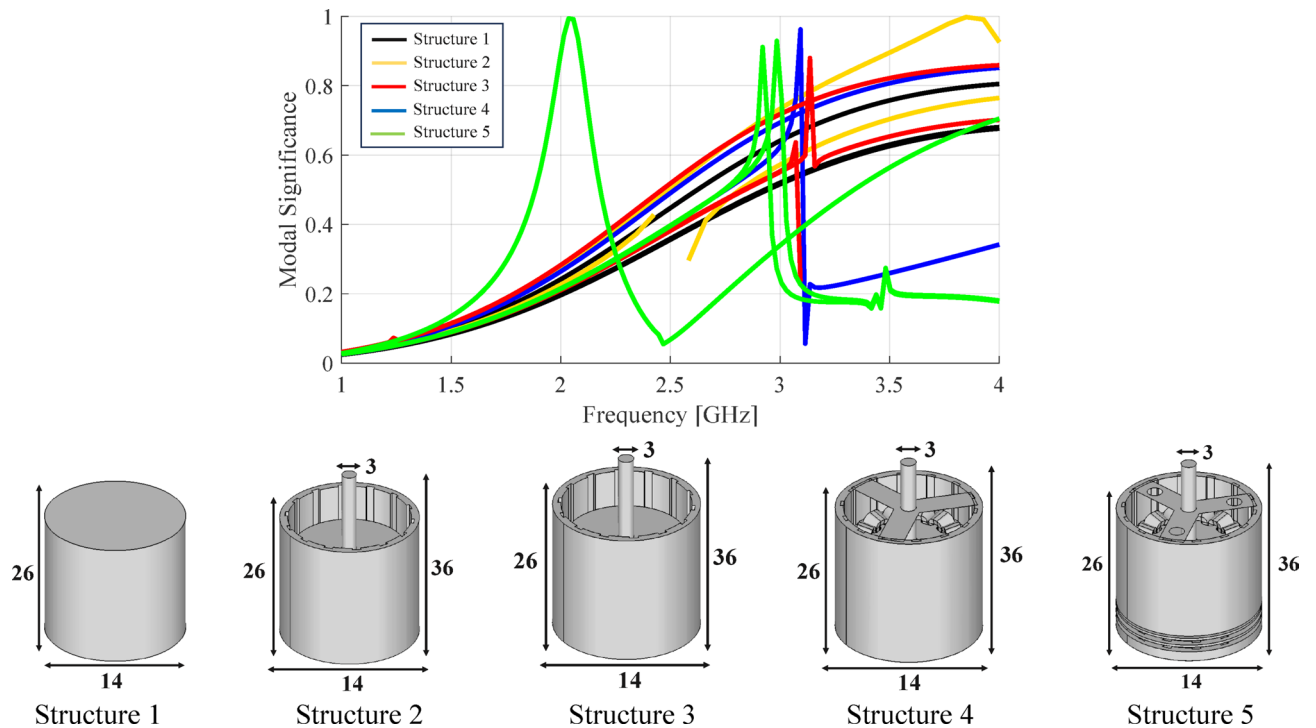


Fig. 2. The influence of motor design parameters on modal significance result.

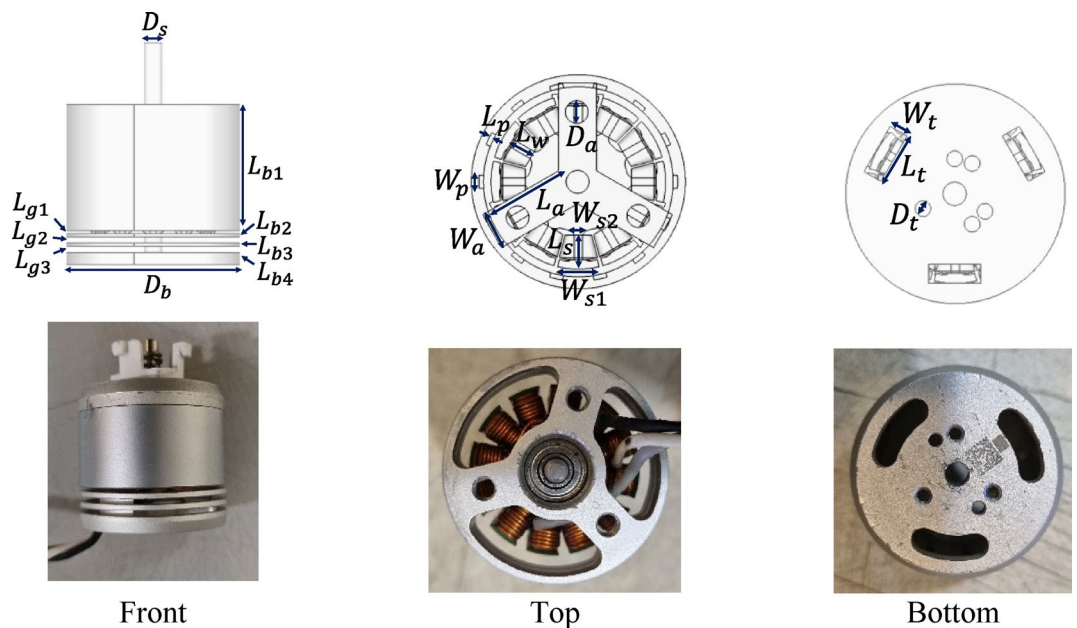
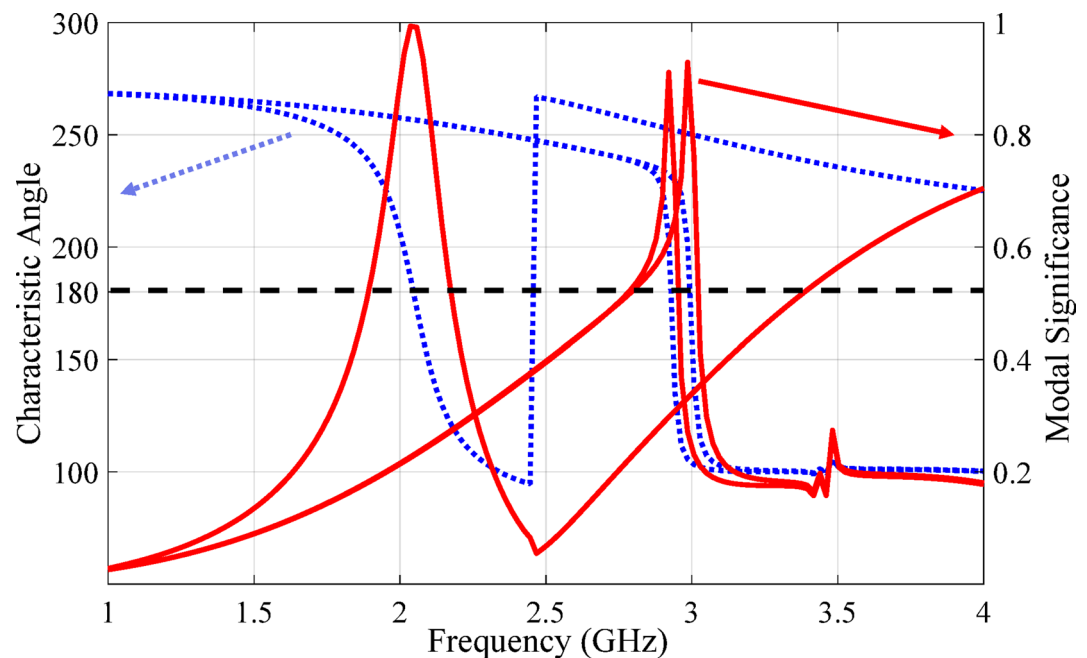


Fig. 3. The motor model applied in this case study.

- For the first mode (2.1 GHz), the structure exhibits maximum vulnerability to theta-polarized radiation incident at theta 90. It exhibits negligible susceptibility to phi-polarized waves or radiation from other directions.
- For the second mode (2.92 GHz), the structure shows significant vulnerability in both polarizations depending on the radiation direction:
 - Theta polarization exhibits maximum coupling at theta 0 and phi 0.
 - Phi polarization shows peak susceptibility at theta 0 and phi 90.
- For the third resonant mode (2.98 GHz), the structure demonstrates critical vulnerability in both polarization states with distinct directional dependence:
 - Theta polarization shows peak EMI coupling at theta 0 and phi 90.

Parameters	Value	Parameters	Value	Parameters	Value
L_{b1}	20.5	L_w	3	W_a	5
L_{b2}	0.5	L_a	10.7	W_t	2.5
L_{b3}	0.5	L_s	8.5	W_p	1.76
L_{b4}	2	L_t	8.75	D_b	28
L_{g1}	0.5	L_p	0.6	D_s	3
L_{g2}	1	W_{s1}	5.5	D_a	3
L_{g3}	1	W_{s2}	1.2	D_t	2

Table 2. The motor model dimensions (Unit: mm).**Fig. 4.** The motor model modal significance and characteristic angle.

- Phi polarization exhibits maximum susceptibility at theta 0 and phi 0.

These observations highlight the different ways in which the structure responds to EMI at various frequencies and polarizations.

To validate the results of the CMA (Computational Magnetohydrodynamics Analysis), a full-wave simulation was conducted to examine surface current excitation:

- **Case 1:** Surface current analysis under fixed frequency while varying the radiation direction and polarization, as illustrated in Fig. 6.
- **Case 2:** Surface current analysis under variable frequency while maintaining constant radiation direction and polarization, as presented in Fig. 7.

As observed in Fig. 6, the surface current distribution on the motor structure was analyzed under varying wave directions and polarizations at 2.1 GHz. Notably, the surface current excitation exhibited peak intensity when the incident wave was oriented at theta 90 with theta polarization. Consequently, the CMA analysis presented in Fig. 5 is confirmed, demonstrating that radiation in the optimal direction and polarization for Mode 1 has the greatest impact on the motor structure. Since Modes 2 and 3 are close in frequency, distinguishing between their effects is challenging. The proximity of these frequency modes makes it difficult to differentiate their individual impacts.

From a frequency perspective, Fig. 7 corroborates the findings presented in Fig. 4, where CMA was employed to identify the resonance frequency. In this simulation, the wave is theta-polarized (θ) and incident at theta 90, with both propagation direction and polarization held constant. As depicted in Fig. 7, radiation at 2.1 GHz, where Mode 1 exhibits resonance according to CMA analysis, generates the highest surface current density excitation particularly in the area where the wires connect to the stator, which shows a higher susceptibility to damage. A similar result is observed for Modes 2 and 3.

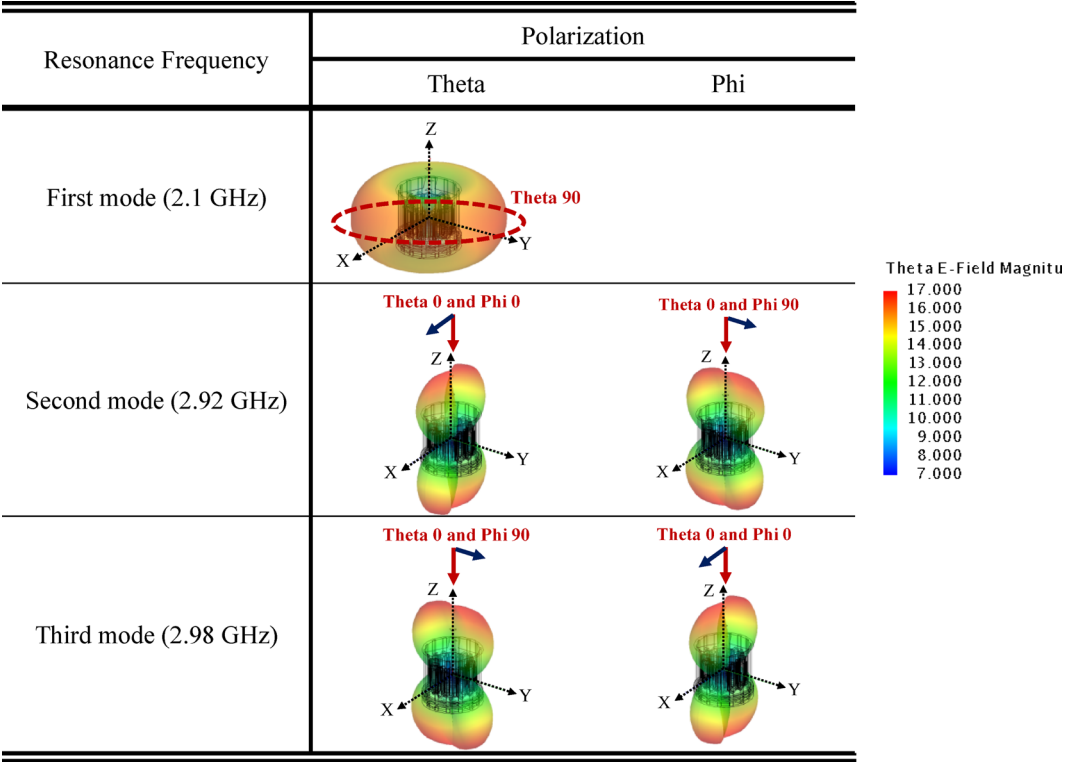


Fig. 5. Radiation pattern of the motor in different modes.

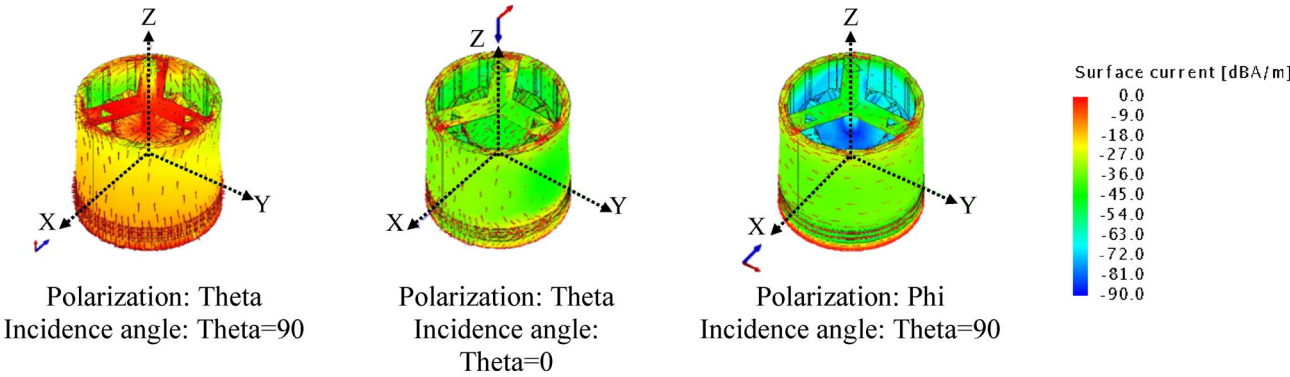


Fig. 6. Surface current density on the motor structure at a frequency of 2.1 GHz for different incident angles and polarization.

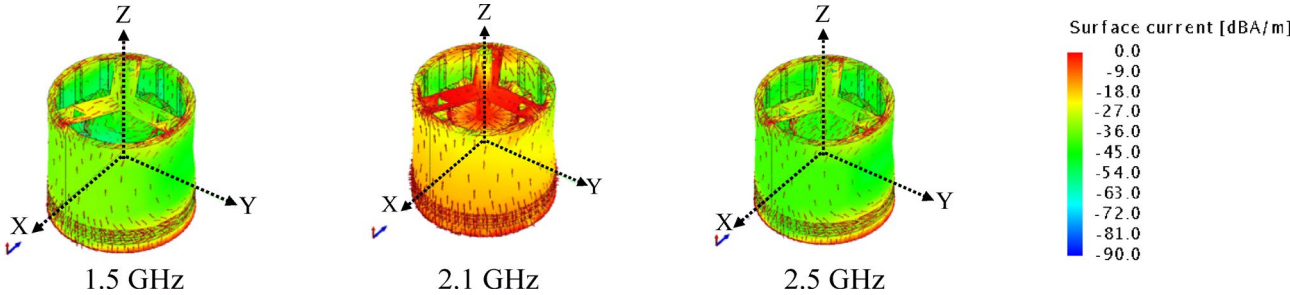


Fig. 7. Validation of the resonance frequency of CMA analysis through Full Wave simulation.

Frequency (GHz)	Direction	Polarization	Field Strength (V/m)
2.1	Theta = 90	Theta	390
2.45	Theta = 90	Theta	1855
2.92	Theta = 0 & Phi = 0	Phi	650
2.98	Theta = 0 & Phi = 0	Theta	1290

Table 3. The minimum field strength that could potentially damage the motor.

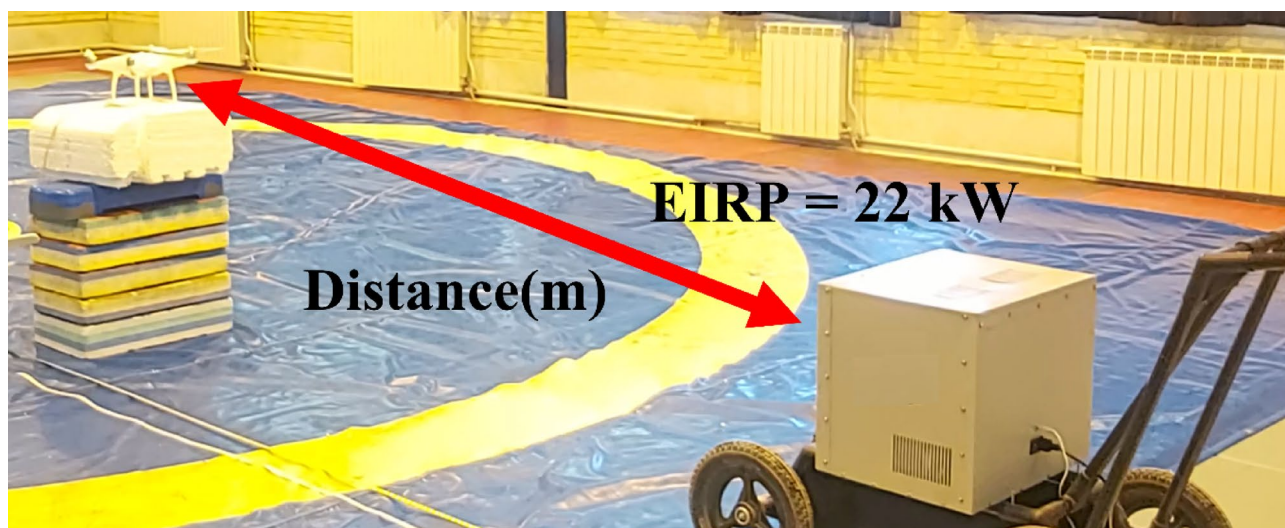


Fig. 8. A high-power wave radiation device operating at a frequency of 2.45 GHz with an EIRP of 22 kW in continuous wave mode, used for irradiating the phantom.

Using near-field analysis, radiation was conducted in the direction and polarization optimal for the three aforementioned modes. Ultimately, radiation was performed at the optimal direction, polarization, and frequency for each of the three modes. Given that the motor's wire connections are made to the stator, power density in the central region of the motor was specifically examined. The minimum field strength for each mode that could potentially damage the motor is presented in Table 3. These results are derived considering that the maximum allowable voltage for the Phantom 4 drone motor is 17.4 volts¹⁸. As evidenced by the simulation results, the minimum field strength required to induce motor failure under theta-polarized irradiation at 2.1 GHz (incidence angle theta 90) was determined to be 390 V/m. This threshold represents the critical EMI exposure level where the induced stator voltage reaches the Phantom 4's maximum rated limit of 17.4 V. Additionally, as shown in Fig. 7, at a frequency of 2.1 GHz, there is a greater accumulation of surface current on the motor windings under theta polarization and an incidence angle of 90 degrees compared to the frequency of 2.45 GHz. With reference to the results obtained in Table 3, at 2.45 GHz, the motor is vulnerable at a field strength of 1855 V/m, indicating a significant difference in susceptibility between the two frequencies.

According to the results, radiation in the direction, polarization, and frequency that excite Mode 1 has the greatest effect on the motor structure.

Experimental measurements

The study evaluated the susceptibility of BLDC motors (outrunner type), which are more widely used in drones, with the DJI Phantom 4 motor serving as the primary case study. The motor specifications are summarized in Table 1, which includes dimensions for the stator and rotor, as well as the number of slots and poles.

EMI testing was performed in a controlled laboratory environment. As shown in Fig. 8, a high-power electromagnetic source consisting of two 2M246 magnetron tubes connected to a horn antenna was employed. This setup provided an effective isotropic radiated power (EIRP) of approximately 22 kW at 2.45 GHz. The distance between the source and the motor was varied (3 m, 2.5 m, 1.5 m, 1 m, and 0.6 m) to assess the impact of field strength on motor performance.

At a distance of 3 m, we observed changes in the sound of motor rotation, and the rotational speed was affected by the radiated field, causing the phantom to fall during operation. This effect intensified as the distance to the source decreased. At 0.6 m, all four motors of the phantom shut down and did not restart; inspection revealed that the motors burned out at this distance.

While the electric field intensity at various distances from a source with EIRP \approx 22 kW is presented in Fig. 9, it is important to note that we could not reduce the distance below 0.6 m. Doing so would have placed the field outside the far-field region, compromising the reliability of our test results. This figure visually illustrates the

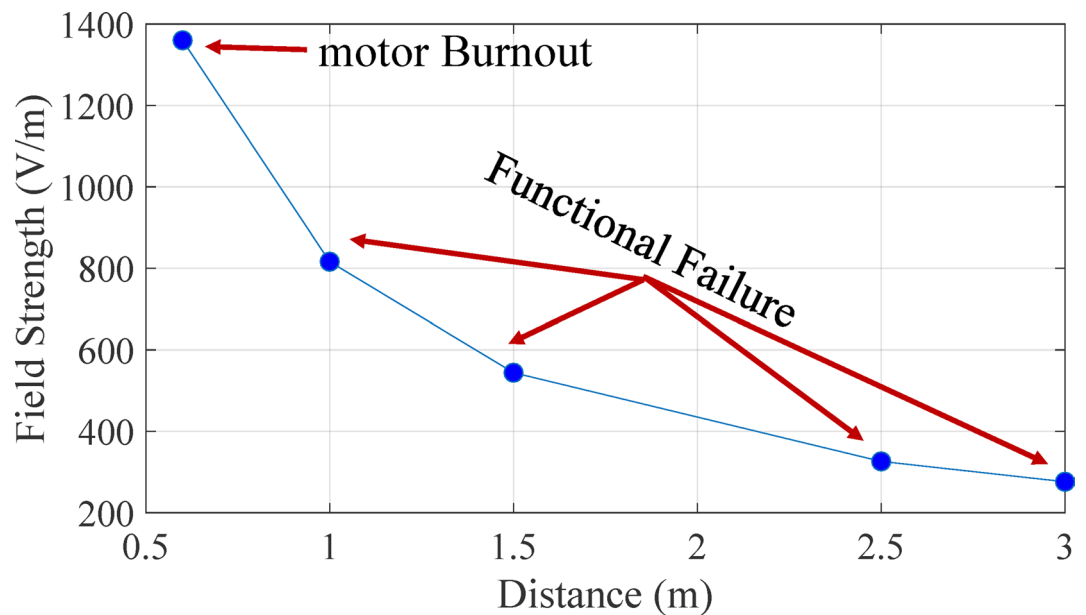


Fig. 9. Electric field intensity at various distances from a source with EIRP \approx 22 kW.

relationship between electric field strength and distance from the radiation source, highlighting key observations such as functional failure and motor burnout.

Due to the inability to use measurement devices during high-power electromagnetic (microwave) radiation without interfering with their functionality, the evaluation of the DC motor's performance was limited to observable changes. At lower field intensities, the motor exhibited audible and visual signs of degradation, such as changes in sound and reduced speed, causing the drone to lose stability and crash. At higher intensities, the motors completely shut down and could not be restarted, indicating irreversible damage. Since external instruments could not be shielded from the radiation, direct observation of the motor's behavior became the only feasible method to assess the impact of the radiation, providing critical insights into its effects on motor functionality.

Although our tests were limited to 2.45 GHz, the insights gained remain invaluable. While Table 3 shows that direct motor damage requires a minimum field strength of 1855 V/m at 2.45 GHz, Fig. 9 reveals that the measured field intensity at the test distance reached only 1360 V/m. As demonstrated in our recent study¹⁹ (analyzing surface current distribution across all drone subsystems under EM radiation), the extended motor wiring plays a critical role in indirect current/voltage induction. These wires effectively harvest energy from the radiated field, creating a secondary pathway for motor burnout. Consequently, the burnout mechanism progresses more gradually under direct power application than through cable-transferred induction. These findings collectively confirm that motor failure results not from direct EM field exposure, but rather from induced currents in the wiring system.

This investigation highlights the critical interplay between electromagnetic field exposure and motor performance, paving the way for future studies to explore a broader frequency range and more sophisticated test setups.

Discussion

The CMA results, including modal significance and radiation patterns, provide critical insights into the physical mechanisms of EMI impact on the motor. Specifically, the high modal significance at frequencies such as 2.1 GHz, 2.92 GHz, and 2.98 GHz indicate resonant behavior that amplifies electromagnetic coupling within the motor structure. For instance, Mode 1 at 2.1 GHz, with its dominant radiation pattern at theta 90 degrees and theta polarization, leads to concentrated surface current density excitation on the motor's stator windings, as confirmed by full-wave simulations (see Fig. 6). This localized current induction increases the risk of overheating and eventual burnout in these regions.

Furthermore, the identified radiation patterns at critical frequencies correlate with specific points of vulnerability within the motor. For example, the radiation pattern at 2.92 GHz (theta polarization at theta 0 and phi 0) and 2.98 GHz (phi polarization at theta 0 and phi 90) suggests that electromagnetic energy couples more effectively with the motor's wiring and electronic speed controller connections. This coupling induces additional currents in the wiring, which, as observed in the experimental measurements, exacerbate motor damage compared to direct radiation exposure. The long wires act as antennas, picking up electromagnetic energy and channeling it into the motor, leading to increased voltage and current levels that exceed the motor's operational limits.

By linking the CMA outputs to these physical mechanisms, it becomes clear how specific modes and radiation patterns translate into increased current induction and localized field concentrations. This understanding not

only validates the CMA predictions but also highlights the importance of designing motor systems with EMI resilience in mind, such as shielding critical components or optimizing wiring layouts to minimize induced currents. Future work could further explore these mechanisms by simulating and testing current distributions and field concentrations in more detail, providing a deeper understanding of EMI-induced failures in motor-driven systems.

Conclusion

This study applied Cumulative Modal Analysis (CMA) to investigate the effects of electromagnetic interference (EMI) on motors, particularly in drones. We identified critical resonant frequencies—2.1 GHz, 2.92 GHz, and 2.98 GHz—indicating that Mode 1 at 2.1 GHz presents the highest vulnerability. At this frequency, radiation in a theta direction of 90 degrees with theta polarization can damage the motor at a field strength of 390 V/m.

Due to limited access to high-power sources across multiple frequencies, practical testing was conducted at 2.45 GHz using a 22 kW electromagnetic source. The experiments revealed that motor performance deteriorated as proximity to the source decreased, with complete failure occurring at 0.6 m. Additionally, the wiring connected to the motor significantly contributed to damage, emphasizing the importance of addressing both direct exposure and induced currents. To mitigate these risks, we recommend implementing shielding on the cables, extending over the connection point of the wires to the motor, where the motor windings are particularly vulnerable. This shield can effectively direct interference away from sensitive components and should be grounded to the motor's body to enhance protection against EMI.

This research demonstrates CMA's value in predicting EMI effects, ultimately improving motor reliability and safety in challenging electromagnetic environments. The insights also support further assessments of other drone components, such as sensors and communication systems, against harmful environmental factors.

Data availability

All data generated or analysed during this study are included in this published article.

Received: 6 January 2025; Accepted: 4 June 2025

Published online: 02 July 2025

References

- Lubkowski, G., Lanzrath, M., Lavau, L. C. & Suhrke, M. Response of the UAV Sensor System to HPEM Attacks, 2020 International Symposium on Electromagnetic Compatibility - EMC EUROPE, Rome, Italy, pp. 1–6. (2020).
- Kim, S. et al. Electromagnetic signature of a quadcopter drone and its relationship with coupling mechanisms. *IEEE Access*. **7**, 174764–174773 (2019).
- Kasmi, C. & Lopes Esteves, J. I. E. M. I. Threats for information security: remote command injection on modern smartphones. *IEEE Trans. Electromagn. Compat.* **57**, 1752–1755 (2015).
- Giri, D., Sabath, F. & Hoad, R. *High-power Electromagnetic Effects on Electronic Systems* (Artech House, 2020).
- Maurine, P. Techniques for EM Fault Injection: Equipments and Experimental Results. In Proceedings of the 2012 Workshop on Fault Diagnosis and Tolerance in Cryptography, Leuven, Belgium, 9 September ; pp. 3–4. (2012).
- Hayashi, Y., Homma, N., Mizuki, T., Aoki, T. & Sone, H. Transient IEMI threats for cryptographic devices. *IEEE Trans. Electromagn. Compat.* **55**, 140–148 (2013).
- Trippel, T., Weisse, O., Xu, W., Honeyman, P. & Fu, K. W. A. L. N. U. T. Waging Doubt on the Integrity of MEMS Accelerometers with Acoustic Injection Attacks. In Proceedings of the 2017 IEEE European Symposium on Security and Privacy (EuroSP), Paris, France, 26–28 April ; pp. 3–18. (2017).
- Yan, C., Xu, W. & Liu, J. Can you trust autonomous vehicles: contactless attacks against sensors of self-driving vehicle. *Def. Con.* **24**, 109 (2016).
- Kune, D. F. et al. Ghost Talk: Mitigating EMI Signal Injection Attacks against Analog S sensors. In Proceedings of the 2013 IEEE Symposium on Security and Privacy, San Francisco, CA, USA, 19–22 May ; pp. 145–159. (2013).
- Feenstra, B. et al. Near-field scanning microwave microscopy: measuring local microwave properties and electric field distributions. In Proceedings of the 1998 IEEE MTT-S International Microwave Symposium Digest (Cat. No. 98CH36192), Baltimore, MD, USA, 7–12 June ; Volume 2, pp. 965–968. (1998).
- Hamdalla, M. Z. M. et al. Electromagnetic Interference of Unmanned Aerial Vehicles: A Characteristic Mode Analysis Approach., *IEEE International Symposium on Antennas and Propagation and USNC-URSI Radio Science Meeting*, Atlanta, GA, USA, 2019, pp. 553–554. (2019).
- Harrington, R. F. & Mautz, J. R. *Theory of Characteristic Modes for Conducting Bodies* (IEEE Transactions on Antennas and Propagation, 1971).
- Chen, Y., Wang, Y., Tang, Q., Zhou, H. & Wang, Y. Electromagnetic radiation analysis and synthesize of UAV target with the theory of characteristic modes, *IET International Radar Conference (IET IRC)*, Online Conference, 2020, pp. 902–905,), Online Conference, 2020, pp. 902–905, (2020). <https://doi.org/10.1049/icp.2021.0716>
- Hamdalla, M. Z. M., Caruso, A. N. & Hassan, A. M. Predicting Electromagnetic Interference to a Terminated Wire Using Characteristic Mode Analysis *2020 International Applied Computational Electromagnetics Society Symposium (ACES)*, Monterey, CA, USA, pp. 1–2. (2020).
- Mohanraj, D. et al. A review of BLDC motor: state of art, advanced control techniques, and applications. *IEEE Access*. **10**, 54833–54869 (2022).
- Millett, P. *Brushless Vs Brushed DC Motors: when and why To Choose One Over the Other* (Technical Marketing Engineer at MPS, 2022).
- (2023). <http://www.altair.com/feko>
- Matrice, D. 300 RTK—User Manual. ed (2020).
- Jalali, Z. et al. Predicting EMI in UAVs using characteristic mode analysis: a case study of the DJI Phantom 4. *Sci. Rep.* **15**, 10016 (2025).

Author contributions

P. H. and A. S. conducted the simulations. S. M. H. developed the analysis methodology and validated the simulations. V. M. and J. G. contributed to the analysis of results and experimental measurements. All authors participated in the scientific review of the work and collaboratively wrote the manuscript.

Declarations

Competing interests

The authors declare no competing interests.

Additional information

Correspondence and requests for materials should be addressed to S.M.H.

Reprints and permissions information is available at www.nature.com/reprints.

Publisher's note Springer Nature remains neutral with regard to jurisdictional claims in published maps and institutional affiliations.

Open Access This article is licensed under a Creative Commons Attribution-NonCommercial-NoDerivatives 4.0 International License, which permits any non-commercial use, sharing, distribution and reproduction in any medium or format, as long as you give appropriate credit to the original author(s) and the source, provide a link to the Creative Commons licence, and indicate if you modified the licensed material. You do not have permission under this licence to share adapted material derived from this article or parts of it. The images or other third party material in this article are included in the article's Creative Commons licence, unless indicated otherwise in a credit line to the material. If material is not included in the article's Creative Commons licence and your intended use is not permitted by statutory regulation or exceeds the permitted use, you will need to obtain permission directly from the copyright holder. To view a copy of this licence, visit <http://creativecommons.org/licenses/by-nc-nd/4.0/>.

© The Author(s) 2025